

# Development of a Mesospheric Sodium Laser Beacon for Atmospheric Adaptive Optics

Thomas H. Jeys

■ We have developed laser sources of sodium-resonance radiation based on the sum-frequency mixing of Nd:YAG laser radiation. The sources are suitable for generating a fluorescence spot in the earth's mesospheric sodium layer for use in adaptive optics compensation. Taking into account the sodium fluorescence lifetime, Doppler broadening, hyperfine structure, radiative saturation, optical pumping, and radiation pressure, we can optimize the intensity of the fluorescence by using spectral and temporal tailoring of the laser radiation.

**A**DAPTIVE OPTICS CAN REDUCE atmospheric distortion effects in astronomical imaging if a bright light source (beacon) is available in the area of the sky under study. Although bright stars are an obvious source of light for astronomical studies [1], most of the sky does not contain stars with the requisite brightness for near-infrared or visible-wavelength adaptive optics [2]. Alternatively, it has been suggested that laser backscattering from molecules in the earth's atmosphere (Rayleigh scattering) or from the earth's mesospheric atomic sodium layer (resonance scattering) can provide the beacon for the adaptive optics compensation of atmospheric distortion [3, 4]. In fact, such compensation has been demonstrated with low-altitude Rayleigh scattering of laser light [5]. Although low-altitude Rayleigh scattering can provide much more backscattered signal to an adaptive optics system, the higher altitude of the mesospheric sodium layer reduces the beam divergence of backscattered radiation and makes the light source more starlike; this factor makes sodium fluorescence the preferred method of producing an artificial beacon [6].

A laser system capable of generating the requisite beacon in the earth's mesospheric sodium layer is currently under development at Lincoln Laboratory. Figure 1 illustrates the general concept of this beacon. Laser radiation at  $0.589 \mu\text{m}$  is transmitted into the atmosphere to excite a relatively small region in the sodium layer. Part

of the fluorescence from the laser-excited atoms that travels back to the earth can, after suffering atmospherically induced wavefront distortion, be collected by a telescope equipped with an adaptive optics system. Measurements of the relative phase change over the distorted wavefront can then be used to apply the reverse (conjugate) phase distortions to the surface of a deformable mirror placed in the optical train of the telescope. In this way, light from an astronomical object collected by the telescope and reflected from the deformable mirror will have its atmospheric optical distortions removed. The

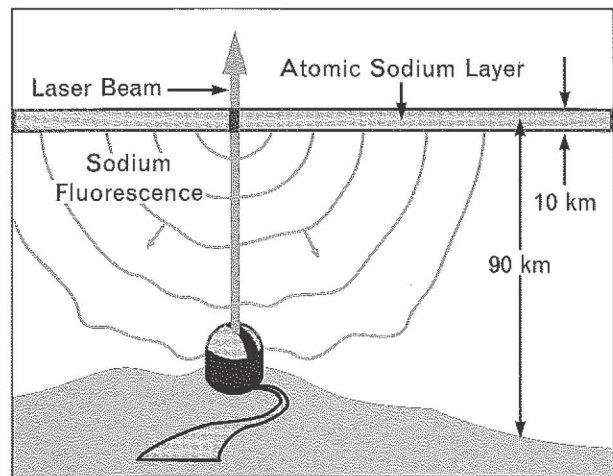


**FIGURE 1.** Schematic showing the use of a mesospheric sodium beacon for atmospheric adaptive optics.

technique therefore enables diffraction-limited astronomical imaging at ground level.

The required beacon brightness is governed by the degree of atmospheric distortion present and by the amount of compensation desired. The distortion is characterized by the atmospheric coherence length  $r_0$ , which varies as the 6/5th power of the radiation wavelength [7]. In order to determine the wavefront distortion of the radiation, one must measure the wavefront tilt for each coherent subaperture with a diameter  $d$  less than or equal to  $r_0$  over the entire telescope aperture. Under good observation conditions,  $r_0$  is  $15 \pm 5$  cm at a wavelength of  $0.5 \mu\text{m}$  and  $79 \pm 27$  cm at a wavelength of  $2 \mu\text{m}$  [8].

The number of detected photons per subaperture  $N_{pe}$  required to correct a telescope equipped with a Hartmann wavefront sensor [9] for a photon-plus-sensor-noise-limited Strehl ratio  $S$  is given by [10]

$$S = e^{-2\pi^2 \left[ N_{pe}^{-1} + 4N_{rms}^2 (G_e N_{pe})^{-2} \right] \left[ 1 + (d/r_0)^2 \right]}$$

where  $N_{rms}$  is the root-mean-square number of sensor noise electrons,  $G_e$  is the detector gain, and the Strehl ratio is the ratio of the actual peak image intensity to the diffraction-limited peak image intensity. For a charge-coupled device (CCD) wavefront sensor with  $N_{rms} = 20$  and  $G_e = 1$ , and for  $d = r_0$ , 400 photons must be detected per subaperture to achieve a Strehl ratio of 0.61.

If we assume that the wavefront sensor has a photon-detection efficiency of 0.8 [11] and the adaptive optics system has an optical throughput of 0.5, then 400 detected photons per subaperture will correspond to  $N_{sub} = 1000$ , where  $N_{sub}$  is defined as the number of received photons per subaperture. (Note: The optical throughput of the experiment described in Reference 5 was only about 0.2 to 0.3. However, the adaptive optics system used was more complex than required for astronomical applications, and the authors of Reference 5 estimate that throughputs of 0.5 should be possible.) The received photons must come from a spot in the sodium layer with a diameter  $D$  less than that resolvable by a subaperture; i.e.,  $D \leq (2.44\lambda/d)R$ , where  $\lambda$  is the wavelength of sodium-resonance radiation and  $R$  is the altitude of the sodium layer [12]. Thus, for  $d = 15$  cm, the maximum  $D$  is 86 cm. Therefore, the laser beam must generate about  $N_{sub} = 1000$  backscattered photons

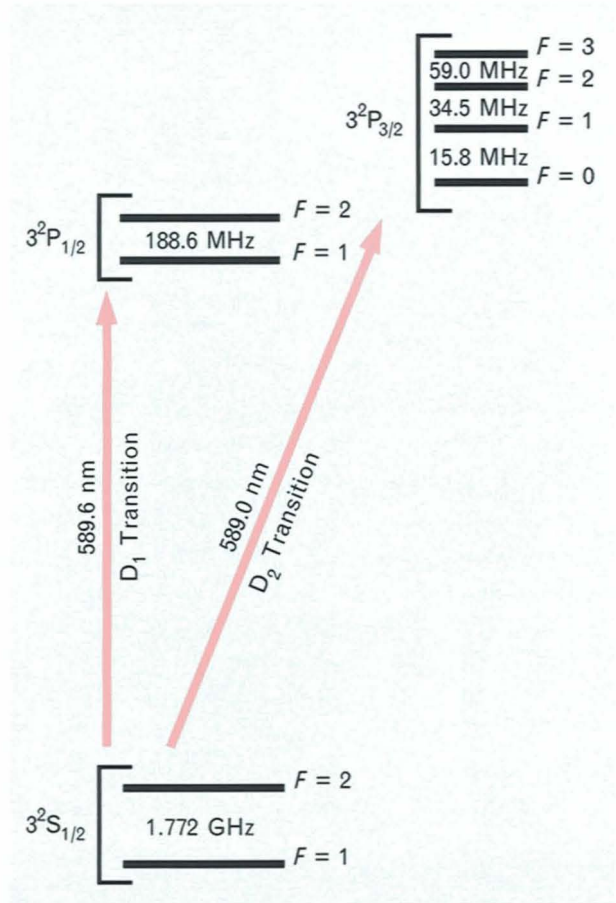


FIGURE 2. Diagram of the  $3^2S_{1/2}$ ,  $3^2P_{1/2}$ , and  $3^2P_{3/2}$  sodium energy levels.

per subaperture at ground level from an area in the sodium layer  $A_{Na} \approx \pi(D/2)^2$  in a time less than the time between changes in the atmospheric optical distortion (1 to 10 msec).

The power, spectral, and temporal requirements of the laser beacon are best understood after reviewing the physics of the interaction of sodium atoms with the resonance radiation.

### Atomic Sodium

Atomic sodium has 11 electrons of which all but one are in closed shells. The single valence electron has a principal quantum number of 3, an orbital-angular-momentum quantum number of 0, and a spin-angular-momentum and total-electron-angular-momentum quantum number of  $S = J = 1/2$ . Naturally occurring sodium is composed of virtually 100% one isotope, which has a nuclear-spin-angular-momentum quantum

number  $l = 3/2$ . The total angular momentum of the ground-state sodium atom is the sum of the total electron angular momentum ( $J = 1/2$ ) and the nuclear-spin angular momentum ( $I = 3/2$ ). The total-angular-momentum quantum number can take on values of either one ( $F = I - J$ ) or two ( $F = I + J$ ). The magnetic interaction between the electron and nuclear magnetic dipole moments cause these two different total-angular-momentum states to have different energies. The state with total-angular-momentum quantum number  $F = 2$  lies above the state with  $F = 1$  by an energy of 1.772 GHz [13]. The spectroscopic notation for the ground states is  $3^2S_{1/2}$ .

The first excited state of sodium also has a principal quantum number of 3 but it has an electron-orbital-angular-momentum quantum number of 1. The combination of electron spin and orbital angular momentum results in two possible total-electron-angular-momentum quantum numbers  $J = 1/2$  and  $3/2$ . The interaction between the electron-spin magnetic moment and the electron-orbital magnetic moment results in the two states ( $J = 1/2$  and  $3/2$ ) being separated in energy by about 520 GHz. The upper state ( $J = 3/2$ ) can be excited by radiation with a wavelength of about  $0.5890 \mu\text{m}$  while the lower state ( $J = 1/2$ ) can be excited by a wavelength of about  $0.5896 \mu\text{m}$ . The interaction of the total electron magnetic moment with the nuclear magnetic moment causes a further splitting of both the  $J = 1/2$  and  $3/2$  states. The  $J = 1/2$  state is split into two hyperfine states (total-angular-momentum quantum numbers  $F = 1$  and  $2$ ) with a separation of 188.6 MHz [13]. The spectroscopic notation for the  $J = 1/2$  excited states is  $3^2P_{1/2}$ . The  $J = 3/2$  state is split into four hyperfine states (quantum numbers  $F = 0, 1, 2,$  and  $3$ ) with separations of 15.8, 34.5, and 59.0 MHz, respectively [13]. The spectroscopic notation for the  $J = 3/2$  excited states is  $3^2P_{3/2}$ . An energy-level diagram for the ground state ( $3^2S_{1/2}$ ) and first excited states ( $3^2P_{1/2}$  and  $3^2P_{3/2}$ ) of atomic sodium is shown in Figure 2.

The radiative lifetime  $\tau$  due to spontaneous emission of an atom in either of the first excited states is 16 nsec. This finite lifetime results in an uncertainty in the energy of each of the hyperfine states:  $\Delta v_n =$  the natural linewidth  $= 1/(2\pi\tau) = 10$  MHz. The normalized absorption profile for low excitation probabilities for a

radiative transition from one of the ground-state hyperfine energy levels to one of the excited-state hyperfine levels is shown in Figure 3(a). This absorption profile is referred to as being *homogeneously broadened* because each atom has the same profile and the same center

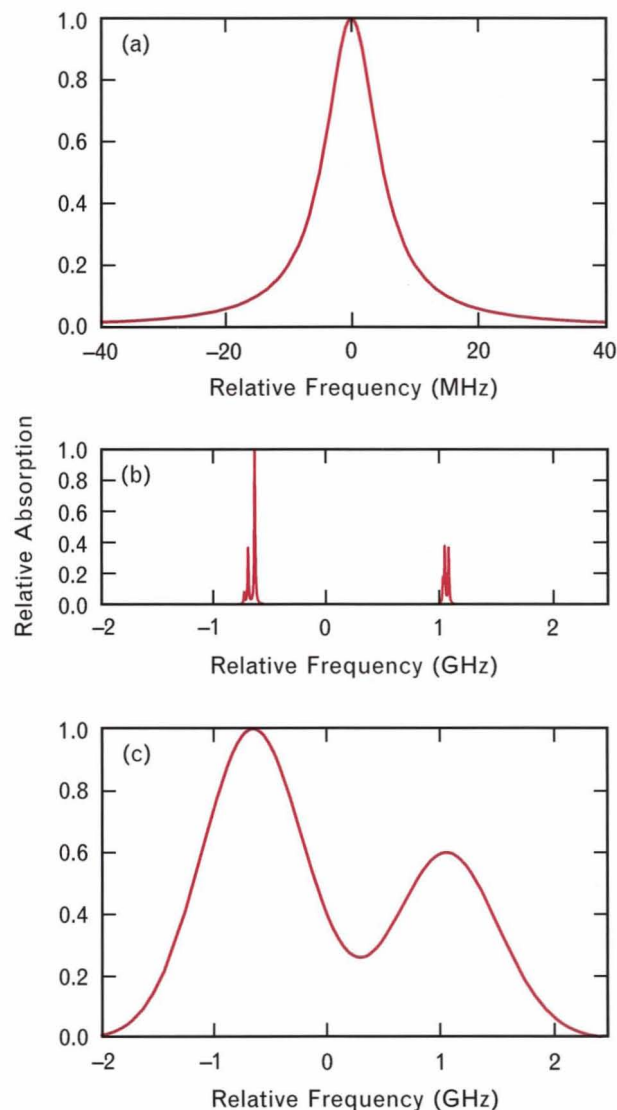


**FIGURE 3.** Sodium  $D_2$  absorption profiles (the  $D_2$  transition occurs between the  $3^2S_{1/2}$  and  $3^2P_{3/2}$  states, as shown in Figure 2): (a) absorption profile for a single hyperfine transition for a single sodium atom, (b) absorption profile for all of the  $D_2$  hyperfine transitions of a single sodium atom, and (c) absorption profile for the Doppler-broadened mesospheric sodium  $D_2$  transitions. At 200 K the Doppler broadening of each hyperfine transition is 1.07 GHz, and thus the 1.772 GHz separation of the sodium ground-state energy levels is well resolved.

frequency. The relative frequencies for all of the  $3^2S_{1/2}$  to  $3^2P_{3/2}$  hyperfine transitions is shown in Figure 3(b). The  $3^2S_{1/2}$  to  $3^2P_{3/2}$  transitions are preferred for the generation of sodium fluorescence because they collectively have a factor of 2 greater absorption strength than the  $3^2S_{1/2}$  to  $3^2P_{1/2}$  transitions. The  $3^2S_{1/2}$  to  $3^2P_{3/2}$  transitions also have better optical-pumping characteristics (discussed in the section "Optical Pumping").

### Mesospheric Environment

The kinetic and chemical dynamics of the mesospheric atomic sodium layer have been studied for many years by lidar techniques. Believed to be principally the result of meteoric ablation, the sodium layer occurs at an altitude of about 90 km and has an average thickness of about 10 km, a column density of around  $5 \times 10^{13}$  atoms/m<sup>2</sup>, and a temperature of about 200 K [14, 15]. The range of velocities of the sodium atoms characterized by this temperature corresponds to a range of frequency shifts for the homogeneous absorption profiles of the sodium atoms (Doppler broadening) of 1.07 GHz full width at half maximum (FWHM). The superposition of all of the  $3^2S_{1/2}$  to  $3^2P_{3/2}$  Doppler-broadened hyperfine absorption profiles is shown in Figure 3(c). The Doppler-broadened absorption profile is referred to as *inhomogeneously broadened* because different velocity atoms have different center absorption frequencies. The combined ground- and excited-state hyperfine-level energy separations and the Doppler broadening result in an absorption profile with  $\Delta\nu_D = 3$  GHz FWHM. Because the mesospheric sodium column density per natural linewidth of 10 MHz is  $\sim 1.7 \times 10^{11}$  atoms/m<sup>2</sup> and the single-atom absorption cross section is  $1.7 \times 10^{-13}$  m<sup>2</sup>, only about 3% of vertically propagating resonance radiation is absorbed and reradiated by the sodium layer.

From an altitude of 85 to 95 km, the atmospheric gas density varies from  $1.7 \times 10^{20}$  to  $2.9 \times 10^{19}$  molecules/m<sup>3</sup> and the mean time between collisions of sodium atoms with atmospheric gas molecules varies from 27 to 155  $\mu$ sec [16]. These collisions redistribute the velocities and consequently the frequency shifts of the sodium atoms within the Doppler-broadened absorption profile, and the collisions limit the effects of radiation pressure (see the section "Radiation Pressure").

The 90-km altitude of the mesospheric sodium layer is a very small fraction of the earth's radius, and thus the

magnetic field at the sodium layer is essentially the same as that at the earth's surface. This  $\sim 0.5$ -G magnetic field produces a precession of the sodium magnetic moment at the Larmor frequency of 0.35 MHz around the direction of the magnetic field. This precession of the magnetic moment adversely affects the optical-pumping process (see the section "Optical Pumping").

### Radiative Saturation

During operation, radiative saturation of the sodium vapor will limit the performance of the sodium beacon [17]; i.e., as the intensity of sodium-resonance radiation increases, the resonance fluorescence will not increase indefinitely. Instead, stimulated emission will become the dominant atomic deexcitation mechanism, and the amount of fluorescence radiation will saturate.

We can analyze the problem of radiative saturation in a general way. Although the normal operating condition is pulsed, for the sake of simplicity we will assume that the sodium vapor is illuminated continuously. Under continuous excitation, the fraction  $f$  of sodium atoms in the excited state at any time can be written as [18]

$$f = \frac{1}{2} \left( 1 + \frac{I_s}{I} \right)^{-1}, \quad (1)$$

where  $I_s$  and  $I$  are the saturation and incident intensities, respectively. The saturation intensity for single-frequency radiation is about 63 W/m<sup>2</sup> [19]. At the saturation intensity, one-fourth of the on-resonance atoms are promoted to the excited state, thus reducing the relative absorption by a factor of 2. Further increases in the amount of resonance radiation produce decreasing amounts of additional absorption and, consequently, of emission. The maximum possible fluorescence is obtained (for time scales long compared to the radiative lifetime of 16 nsec) at radiation intensities many times the saturation intensity, with an average of one-half of the atoms in the excited state. On average, therefore, each atom will emit a fluorescence photon every two radiative lifetimes. The angular distribution of the fluorescence depends on the details of the excitation process, but it is at most 1.5 times higher in the backward direction than would result from a purely isotropic distribution [20]. Thus the maximum backscattering rate is  $(1 \text{ photon/atom}/32 \text{ nsec}/4\pi \text{ sr}) \times 1.5 = 3.73 \times 10^6$  photons atom<sup>-1</sup> sec<sup>-1</sup> sr<sup>-1</sup>.

An estimate of  $t_{\min}$ , the minimum time required to generate  $N_{\text{sub}}$  photons per subaperture, is

$$t_{\min} = 2\tau n_{\min}, \quad (2)$$

where  $\tau$  is the sodium radiative lifetime of 16 nsec and  $n_{\min}$  is the minimum number of times that each sodium atom must spontaneously radiate a photon.

The number of photons received per subaperture  $N_{\text{sub}}$  can be found from the following equation:

$$N_{\text{sub}} = \rho A_{\text{Na}} n_{\min} \frac{A_{\text{sub}}}{4\pi R^2} 1.5T, \quad (3)$$

where  $\rho$  is the sodium column density,  $A_{\text{Na}}$  is the area of illuminated sodium  $= (\pi/4)(2.44\lambda R/d)^2$ ,  $\lambda$  is the sodium-resonance wavelength  $= 0.589 \mu\text{m}$ ,  $R$  is the altitude of the sodium layer,  $d$  is the subaperture diameter,  $A_{\text{sub}}$  is the area of the subaperture  $= \pi d^2/4$ , and  $T$  is the atmospheric transmission.

Solving Equation 3 for  $n_{\min}$  and eliminating  $A_{\text{Na}}$  and  $A_{\text{sub}}$  leads to

$$n_{\min} = \frac{16N_{\text{sub}}}{1.5\pi(1.22\lambda)^2 \rho T}.$$

Thus for a sodium column density of  $5 \times 10^{13} \text{ m}^{-2}$  and an atmospheric transmission of 80%, 1000 photons will be received per subaperture if each atom emits  $n_{\min} = 164$  photons. From Equation 2, the minimum time  $t_{\min}$  required to emit these photons is 5.3  $\mu\text{sec}$ .

An estimate of the laser energy per natural linewidth required for each atom to emit  $n_{\min}$  photons is found by setting

$$n_{\min} = \frac{dn}{dt} t_1, \quad (4)$$

where  $t_1$  is the laser pulse length, and  $dn/dt$  is the rate at which an atom emits photons  $= f/\tau$ . The quantity  $f$  can be found from Equation 1.

Equations 1 and 4 can be solved for the required laser energy per natural linewidth transmitted from the ground,  $E = It_1 A_{\text{Na}} T^{-1}$ , yielding

$$E = I_s t_{\min} A_{\text{Na}} \left(1 - \frac{t_{\min}}{t_1}\right)^{-1} T^{-1}.$$

The total transmitted energy required for each atom in the Doppler-broadened profile to emit  $n_{\min}$  photons is given by the equation

$$E_D = \frac{\Delta v_D}{\Delta v_n} I_s t_{\min} A_{\text{Na}} \left(1 - \frac{t_{\min}}{t_1}\right)^{-1} T^{-1},$$

where  $\Delta v_D$  is the Doppler-broadened absorption width  $= 3 \text{ GHz}$ , and  $\Delta v_n$  is the natural linewidth  $= 10 \text{ MHz}$ .

For laser pulse lengths  $t_1$  that are long compared to  $t_{\min}$ ,  $E_D$  is independent of the pulse length and has its minimum value. For  $t_{\min} = 5.3 \mu\text{sec}$  and a subaperture diameter of  $d = 15 \text{ cm}$ , the minimum transmitted energy  $E_{D\min} = 73 \text{ mJ}$ . (As stated earlier, the subaperture diameter scales as the 6/5th power of the imaging wavelength and thus  $E_{D\min}$  scales as the  $-12/5$ th power of this wavelength. At an imaging wavelength of  $2 \mu\text{m}$ ,  $r_0 = d = 79 \text{ cm}$  and thus  $E_{D\min} = 2.6 \text{ mJ}$ .)

So far we have assumed that the laser has a spectral output that can access all of the sodium atoms over the full Doppler-broadened absorption profile. This capability requires that the laser radiation contain spectral components spaced at around or less than intervals of the sodium homogeneous linewidth of 10 MHz. Such spacing, however, is usually difficult to obtain from a laser cavity. For example, a conventional laser source with a cavity length of 1.5 m can support output frequencies spaced only as close as 100 MHz. If this laser has a temporal coherence greater than 100 nsec, then on resonance it can directly access only about 1/10 of the available sodium atoms; thus this laser must have a pulse length 10 times longer than that of a laser with 10-MHz frequency intervals to generate backscattered photons just as efficiently. But there is a limit to how long the laser pulse can be made. (With external phase modulation of the laser radiation, it should be possible to generate additional frequencies in the laser spectrum so that the radiation can access all of the sodium atoms [21].)

The maximum laser pulse length depends on the geometry of the laser transmitter and backscattered-photon receiver. The transmitter and receiver can be configured with either separate apertures (bistatic system) or a single aperture (monostatic system). In a bistatic system the beacon laser can be operated either continuously or in a pulsed mode. In either mode the signal integration time and the effective laser pulse length must be less than the time between changes in the atmospheric optical distortion. The bistatic transmitter and receiver could be placed far enough apart so that the receiver telescope does not collect atmospheric Rayleigh scattering from

the transmitted laser radiation, thus making time gating unnecessary.

We have concentrated our efforts on the development of a laser beacon for a monostatic adaptive optics system. The principal advantage of a monostatic system is that the transmitted laser radiation traverses roughly the same path through the atmosphere as the backscattered sodium fluorescence, and thus the centroid of the beacon image does not wander around in the field of view of the telescope.

A monostatic system must, however, contend with Rayleigh backscattering. The corruption of the sodium fluorescence signal by low-altitude Rayleigh backscattering limits the monostatic beacon laser to pulsed operation. The laser pulse length must be less than the 250  $\mu\text{sec}$  set by twice the transit time of light from the upper altitude of Rayleigh scattering (about 40 km) to the lower altitude of sodium scattering (about 80 km). In addition, the round-trip transit time of light from the earth's surface to the upper altitude of the sodium layer (about 100 km) restricts the laser repetition rate to less than 1.5 kHz (Figure 4).

To eliminate the collection of Rayleigh-scattered signals, the backscattered signal must be time gated. The sodium backscattered signal can then be integrated over multiple laser pulses as long as the atmosphere does not change during the integration time.

If we limit the time interval during which the wavefront sensor must detect the backscattered photons from the sodium layer to a laser pulse length of  $t_1$  seconds and if the laser system generates frequencies only every  $\Delta\nu_1 > \Delta\nu_n$ , then the required transmitted laser energy can be calculated as follows:

$$E'_D = \frac{\Delta\nu_D}{\Delta\nu_n} I_s t_{\min} A_{\text{Na}} \left( 1 - \frac{t'_{\min}}{t_1} \right)^{-1} T^{-1},$$

where  $t'_{\min} = 2\tau n_{\min}(\Delta\nu_1/\Delta\nu_n)$ .

Thus a laser with a pulse length of 250  $\mu\text{sec}$  and output frequencies every 100 MHz over the Doppler-broadened absorption profile must transmit a minimum of about 93 mJ per pulse in order to generate 1000 backscattered photons per 15-cm subaperture.

More sophisticated calculations of laser-induced beacon fluorescence can be divided into two regimes, depending on the temporal characteristics of the radiation. For radiation that changes on a time scale no shorter

than several times the sodium radiative lifetime, simple rate-equation calculations are valid for estimating the level of atomic excitation by the laser radiation. But for short pulses of radiation or for radiation that consists of a train of short pulses such as mode-locked pulses, the optical Bloch equations must be used because the analysis needs to account for the coherence between the light and the atoms [20].

In addition to radiative saturation, optical pumping can strongly affect the amount of energy required in a laser pulse, and, for a laser with frequency intervals  $\Delta\nu_1 \gg \Delta\nu_n$  and intensities per frequency interval  $> I_s$ , radiation pressure can also affect the laser requirements.

### Optical Pumping

For laser illumination times that are long compared to the radiative lifetime, the effects of optical pumping must be considered. Optical pumping produces a change in the atomic-level populations and can cause such ex-

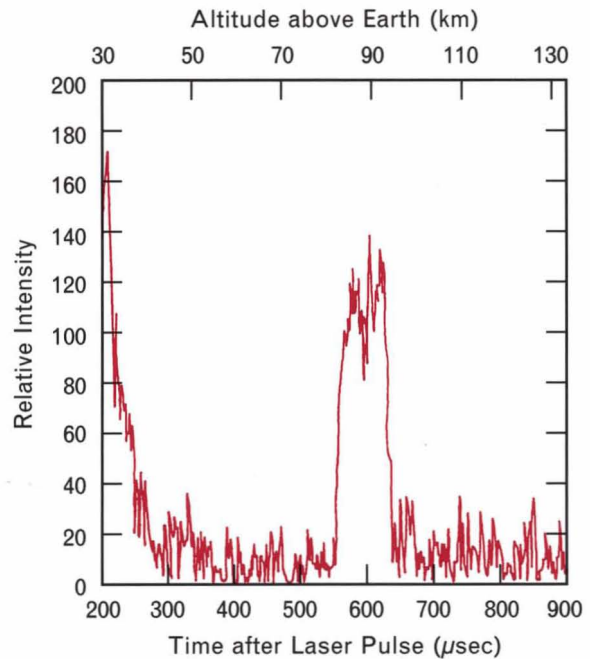


**FIGURE 4.** Sodium-resonance radiation backscattered by the earth's atmosphere. The relative backscattered intensity is plotted versus the elapsed time after a short laser pulse of sodium-resonance radiation is transmitted into the atmosphere. The return signal at times  $< 300 \mu\text{sec}$  is the result of Rayleigh backscattering. The return signal from the mesospheric sodium layer occurs at a round-trip time of  $600 \mu\text{sec}$ . (The data were collected on 25 August 1987.)

treme conditions as either optically induced transparency (which leads to reduced backscattering) or optimum optical pumping (which leads to increased backscattering).

Figure 5(a) shows that optically induced transparency results when a single hyperfine energy level in the 3S ground state of sodium is illuminated with noncircularly polarized radiation. Although the atoms are excited out of just one 3S hyperfine energy level ( $F = 2$ ), they can, in general, decay back to either hyperfine level ( $F = 1$  or  $F = 2$ ). Consequently, after several excitation/decay cycles all of the sodium atoms will reside in the unpumped hyperfine level. The vapor will then be transparent to the laser radiation.

For optimally efficient optical pumping, the atoms should be illuminated with circularly polarized radiation, which will excite both ground states (Figure 5[b]). After several excitation/decay cycles the sodium atoms will have absorbed angular momentum from the radiation field and will reside in the higher angular-momentum hyperfine state ( $F = 2$ ). The sodium absorption profile will then consist of only the  $F = 2$  peak. The earth's magnetic field does, however, compete with the optical-pumping process by causing a precession of the atomic magnetic moment at the Larmor frequency  $\nu_{\text{Larmor}} = 0.35$  MHz, thus allowing optical transitions that would otherwise be forbidden. In the absence of a perturbing magnetic field, about 20 excitation/decay cycles are required for the optical pumping of most of the sodium atoms into the  $F = 2$  ground state with circularly polarized radiation. For  $\nu_{\text{Larmor}} > n_{\text{min}}/(20t_1)$ , the effects of circularly polarized optical pumping diminishes because fewer atoms are pumped into the  $F = 2$  ground state.

From the point of view of minimizing the transmitted laser energy needed to generate  $n_{\text{min}}$  photons per atom, the optimum laser spectral profile is governed by the need to excite predominantly the  $F = 2$  hyperfine level while retaining some laser radiation for excitation of the  $F = 1$  hyperfine level. In the absence of the magnetic field, the optimum laser spectral lineshape is centered close to the  $F = 2$  transition with a linewidth of 1.5 to 2 GHz FWHM [20].

### Radiation Pressure

Radiation pressure on the sodium atoms can substantially change the amount of resonance fluorescence by

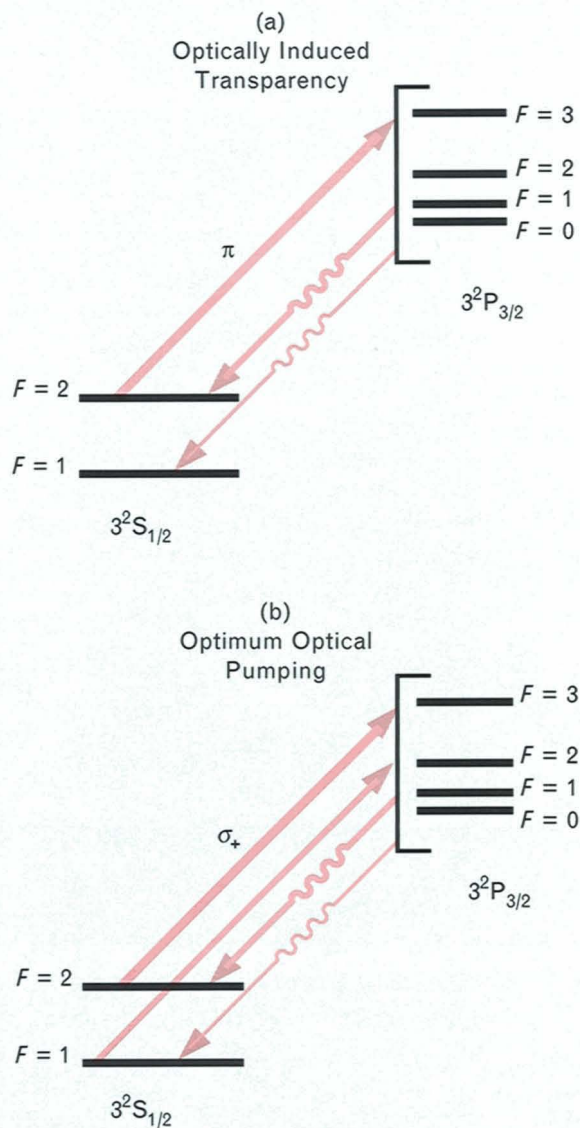


**FIGURE 5.** Sodium energy-level diagram showing two extreme examples of laser-induced optical pumping: (a) linearly polarized light resonant with transitions involving only one hyperfine ground state causes induced optical transparency of the sodium vapor when all of the sodium atoms are pumped to the nonresonant ground state, and (b) circularly polarized light can pump the atom to a state that has the highest efficiency for backscattering of the laser radiation.

altering the longitudinal velocity of the atoms and by pushing them out of resonance. This process is particularly important for single-frequency laser radiation or laser radiation that consists of a comb of frequencies separated by several homogeneous linewidths of

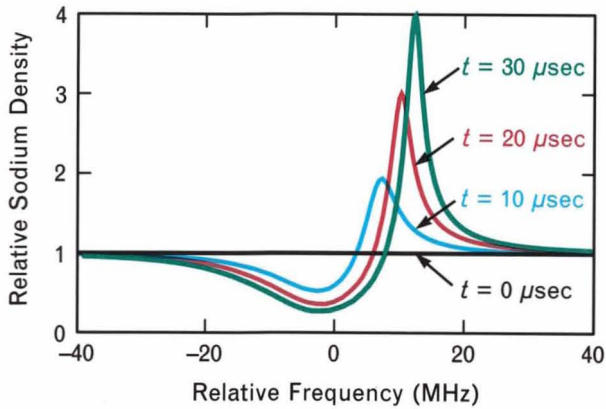


**FIGURE 6.** Resonant radiation pressure on the sodium atoms can push them out of resonance with the radiation. The relative sodium density is plotted as a function of relative frequency over a very narrow range of the Doppler profile. In the absence of radiation pressure, the density is essentially uniform over this frequency interval. Single-frequency saturation intensity ( $63 \text{ W/m}^2$ ) at zero relative frequency pushes the sodium atoms by differing amounts in frequency, depending on  $t$ , the duration of the interaction.

the sodium atom [22].

After an atom absorbs a photon traveling in the direction of the laser beam, the atom radiatively decays by emitting a photon in an arbitrary direction. This process on average causes the atom to absorb one unit of photon linear momentum per absorption/emission cycle, and the change in momentum increases the absorption frequency of the atom by 50 kHz. At the saturation intensity, an atom absorbs a laser photon every 64 nsec, and thus the atom's resonant frequency shifts at a chirp rate of  $50 \text{ kHz}/64 \text{ nsec} = 0.78 \text{ MHz}/\mu\text{sec}$ . As the atom moves out of resonance with the radiation, the frequency chirp decreases. The effect of such radiation pressure due to single-frequency saturation intensity is shown in Figure 6. Note that for increasing interaction times, the sodium atoms are progressively pushed further out of resonance with the exciting radiation.

Collisions between the sodium atoms and background gas molecules will redistribute the atomic velocities and fill the velocity hole created by radiation pressure. These collisions, however, are relatively infrequent, as discussed previously. Therefore, ample time exists for a long laser pulse to push the atoms out of resonance before background-gas collisions can rethermalize the vapor.

The loss in excitation efficiency due to radiation pres-

sure can be overcome by illuminating the sodium vapor with radiation that has spectral content at intervals of the homogeneous absorption linewidth. Then the sodium atoms will be pushed merely from one homogeneous velocity group to another. This spectral content is the same content requirement given earlier for complete excitation over the Doppler profile.

It is also possible, however, to have the radiation pressure work to increase the sodium excitation efficiency of single-frequency laser radiation or of laser radiation that consists of a sparse comb of frequencies by chirping the laser frequencies so that they follow the resonant frequency of the sodium atoms. This technique sweeps the sodium atoms into velocity groups in resonance with the laser radiation, and increases the absorptance of the sodium vapor.

### Laser Systems

Several types of laser systems are capable of generating sodium-resonance radiation. We chose to use a frequency-shifted Nd:YAG solid state laser because it is a reliable laser system that can be scaled to high repetition rates, high pulse energies, and long pulse lengths, and yet can

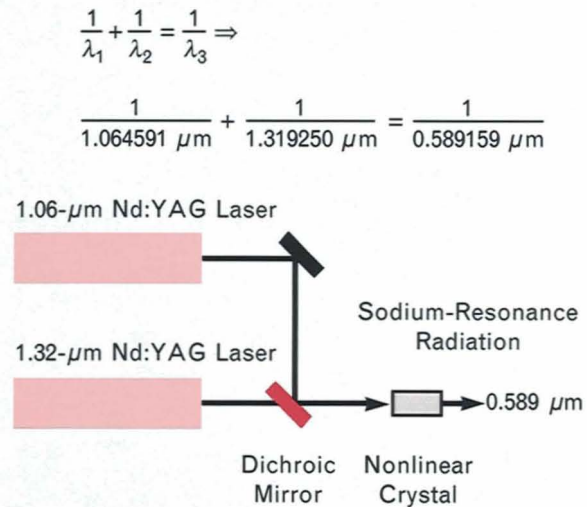


**FIGURE 7.** The Nd:YAG laser system for sum-frequency generation of sodium-resonance radiation. (Nd:YAG is a neodymium-doped garnet crystalline material comprised of yttrium, aluminum, and oxygen— $\text{Nd:Y}_3\text{Al}_5\text{O}_{12}$ .) The exact vacuum wavelength of the emitted sum radiation is given in the equation shown, and this wavelength gives a good match to the sodium  $\text{D}_2$  absorption line.

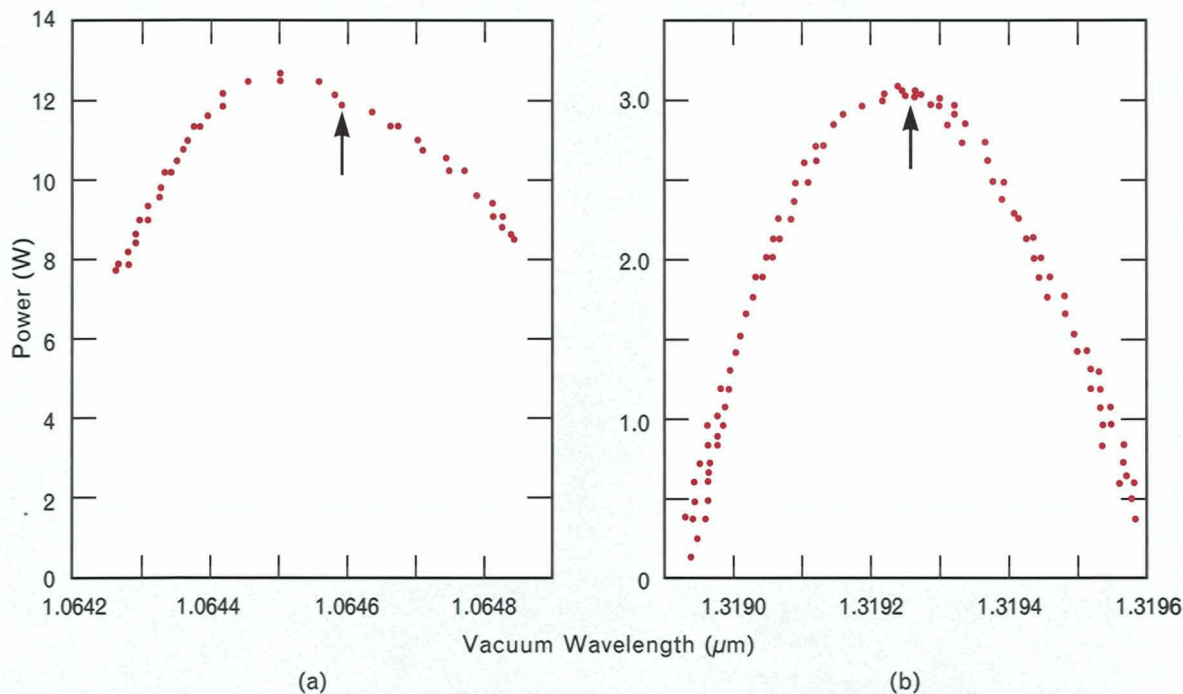


**FIGURE 8.** Tuning curves of (a) 1.06- $\mu\text{m}$  and (b) 1.32- $\mu\text{m}$  Nd:YAG lasers. The absolute wavelengths were measured with a vacuum wavemeter. To eliminate water-vapor absorption lines, which would significantly suppress the long-wavelength end of the tuning curve, the 1.32- $\mu\text{m}$  Nd:YAG laser cavity was purged with nitrogen gas. Sodium-resonance radiation was generated by sum-frequency mixing radiation with the wavelengths indicated by the arrows. The 1.32- $\mu\text{m}$  laser is usually less powerful than the 1.06- $\mu\text{m}$  laser and therefore the former was operated at the peak of its tuning curve.

still maintain near-diffraction-limited beam quality. Moreover, this laser system easily meets the spectral and temporal requirements of the sodium beacon. (Note: Nd:YAG is a neodymium-doped garnet crystalline material comprised of yttrium, aluminum, and oxygen— $\text{Nd:Y}_3\text{Al}_5\text{O}_{12}$ .)

At Lincoln Laboratory, we have generated sodium-resonance radiation by sum-frequency-mixing the output of a 1.06- $\mu\text{m}$  Nd:YAG laser with the output of a 1.32- $\mu\text{m}$  Nd:YAG laser (Figure 7). The lasers are operated at wavelengths very close to the peak of their tuning curves, as indicated by the arrows in Figure 8. Thus it is possible to match the wavelength of the sum-frequency radiation to that of the sodium  $D_2$  absorption wavelength of 0.589  $\mu\text{m}$  [23]. (The  $D_2$  transition occurs between the  $3^2S_{1/2}$  and  $3^2P_{3/2}$  atomic states, as shown in Figure 2.)

We can produce the sum radiation over a 0.3-nm (260-GHz) range that has a peak nearly centered at the

$D_2$  transition and that encompasses the hyperfine and Doppler-broadened sodium absorption profile of 3.5 pm (3 GHz) FWHM. Because the  $D_1$  transition ( $3^2S_{1/2} \rightarrow 3^2P_{1/2}$ ) is nearly 0.6 nm (520 GHz) from the  $D_2$  transition, radiation resonant with the  $D_1$  transition can not be generated. (Note: The  $D_1$  and  $D_2$  transitions could both be reached by using the larger tuning range of a Nd:glass laser, but more fluorescence can be obtained from the  $D_2$  line than from the  $D_1$ .)

We have developed two pulsed laser systems for the generation of sodium-resonance radiation: one system operates at 10 Hz with 0.5 J per pulse and the other operates at 840 Hz with 24 mJ per pulse. Each laser system is composed of both 1.06- $\mu\text{m}$  and 1.32- $\mu\text{m}$  flash-lamp-pumped master oscillators followed by power amplifiers, and each oscillator is linearly polarized and operated with a long pulse length and TEM<sub>00</sub>-mode output. In addition, each oscillator contains an intracavity doubling crystal for the suppression of laser spiking and, for

greater mixing efficiency, each oscillator is mode locked to increase the peak output intensity of the laser.

### Spiking Suppression

Typical long-pulse operation of a Nd:YAG laser will result in pronounced laser spiking during the laser pulse. Laser spiking is caused by the development of laser gain that is much greater than the steady-state, or threshold, gain. The absence of appreciable stimulated emission at the start of laser pumping allows the laser gain to rise substantially beyond the threshold gain. This high initial gain leads to a rapid buildup in the laser radiation intensity, which then depletes the gain and, after a short delay, results in a greatly reduced radiation intensity. The low radiation intensity and continued laser pumping allow the redevelopment of high laser gain, which leads to another intensity buildup. The cycle of low intensity, high gain followed by high intensity, low gain continues through the rest of the laser pulse, with a damping rate dependent on the laser pumping rate and the laser cavity losses. The spiking behavior of a 1.06- $\mu\text{m}$  Nd:YAG laser is illustrated in Figure 9(a).

Laser spiking can be suppressed by an intracavity nonlinear crystal that converts the high-intensity laser spikes into second-harmonic radiation. With such a crystal, the peak intensities of the initial laser spikes are substantially reduced through second-harmonic generation; consequently, they do not drive the laser gain as far below threshold. Thus, the laser spiking behavior damps out at a much higher rate than in the absence of intracavity doubling, and the redevelopment of spiking is suppressed. The effect of the nonlinear crystal on the 1.06- $\mu\text{m}$  laser performance is shown in Figure 9(b).

We can increase the rate of damping of laser spiking by increasing the second-harmonic conversion efficiency. This improvement can be accomplished by increasing the intracavity radiation intensity through decreased output coupling, by using a nonlinear crystal with a high nonlinear coefficient, and by positioning the nonlinear crystal at an intracavity beam waist. Mode locking also increases second-harmonic generation. When a laser is mode locked, the peak power of the radiation increases and second-harmonic radiation is generated with greater efficiency. We have achieved near-critical damping in a mode-locked 1.06- $\mu\text{m}$  Nd:YAG laser. In this case, second-harmonic generation produced only

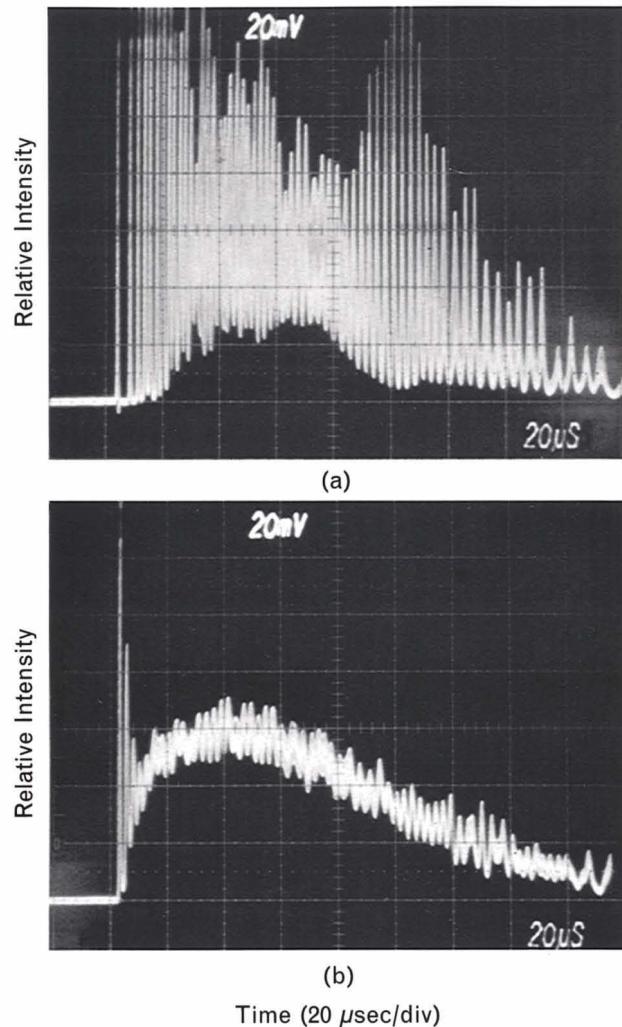


**FIGURE 9.** Oscilloscope photographs of 1.06- $\mu\text{m}$  laser oscillator pulses (a) without intracavity second-harmonic generation, and (b) with intracavity second-harmonic generation.

a 6% loss in 1.06- $\mu\text{m}$  laser pulse energy. We have also achieved similar spiking suppression in a 1.32- $\mu\text{m}$  Nd:YAG laser.

It is important to eliminate the independent spiking behavior of the 1.06- and 1.32- $\mu\text{m}$  lasers to obtain good temporal overlap of the laser pulses for efficient sum-frequency mixing. Therefore, each oscillator cavity in both the 10-Hz and 840-Hz Nd:YAG laser systems contained a nonlinear crystal for suppressing laser spiking through second-harmonic generation [24].

### Efficient Mixing of Low-Peak-Power Radiation

Because of the long pulse lengths required for efficient sodium excitation, the Nd:YAG laser radiation has rela-

tively low peak powers. Efficient mixing of low-peak-power radiation places severe constraints on the nonlinear crystal. To achieve efficient mixing of low-peak-power radiation, we must tightly focus the radiation into the nonlinear crystal to obtain high peak intensities. However, the angular content of the focused radiation must be kept less than the phase-matching angular acceptance of the crystal. The relatively narrow angular acceptance of such crystals as  $\text{KH}_2\text{PO}_4$ ,  $\text{LiIO}_3$ , and  $\text{KNbO}_3$  limits the degree of focusing that can profitably be applied to the pump radiation.

In addition, if the radiation is continuous wave or pulsed with a high duty cycle, then tight focusing results in a high average intensity at the focus. Such intensity can result in substantial local heating of the crystal if there is absorption of even a small fraction of either the incident radiation or the sum-frequency radiation. Local heating of the crystal results in a local temperature gradient, which can adversely affect the sum-frequency mixing efficiency if the gradient across the beam exceeds the phase-matching temperature-acceptance range of the crystal or if the gradient results in mechanical stress to the crystal because such stress can effect the phase-matching process and can result in mechanical damage to the crystal. High average intensities can also result in the creation of photorefractive damage in the crystal at a rate greater than this damage can be thermally dissipated. Consequently, the small temperature-acceptance range, relatively high optical absorption coefficients, and high susceptibility to photorefractive damage of crystals such as  $\text{LiNbO}_3$  and  $\text{KNbO}_3$  severely limit the utility of these materials in high-average-intensity applications.

The 10-Hz Nd:YAG laser system used  $\text{LiIO}_3$  (lithium iodate) for sum-frequency generation. Lithium iodate can sustain high intensities and fluences and generate sum radiation with excellent efficiency. However, lithium iodate has a very narrow angular acceptance for efficient mixing of radiation. This property and the need for substantial focusing of the input radiation required the Nd:YAG laser radiation to have near-diffraction-limited beam quality. We focused the Nd:YAG laser radiation into the lithium-iodate crystal with cylindrical lenses to take advantage of the very different phase-matching angular acceptances of the two orthogonal transverse directions.

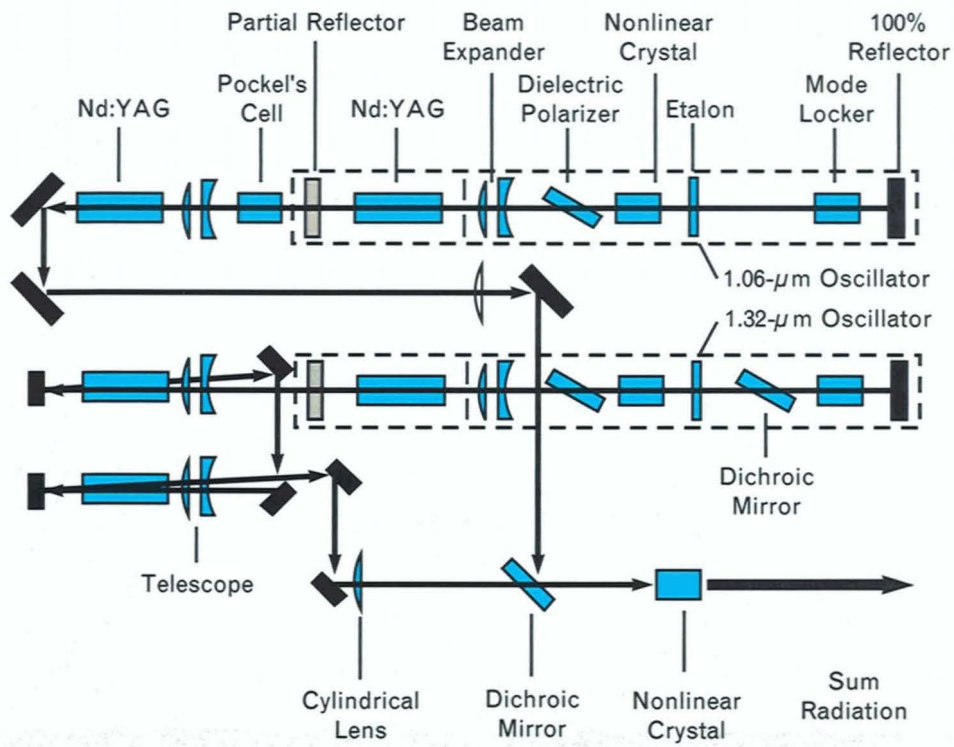
The 840-Hz Nd:YAG laser system had peak powers about 20 times lower than that of the 10-Hz laser system. As a result, it was not possible to focus the laser radiation to sufficiently high intensities for efficient mixing while at the same time keeping the divergence of this radiation within the phase-matching angular acceptance of lithium iodate. Thus we instead used  $\text{LiB}_3\text{O}_5$  (lithium triborate), a relatively new nonlinear material, for sum-frequency mixing. Lithium triborate has several advantages for efficient mixing of low-peak-power, high-duty-cycle Nd:YAG laser radiation. With temperature tuning, lithium triborate can be phase matched to have a very large angular acceptance. But in contrast to other temperature-tunable crystals, lithium triborate has a relatively large phase-matching temperature-acceptance range [25]. The most interesting characteristic of lithium triborate for high-average-intensity applications is the low optical absorption coefficients, which minimize thermal gradients and their deleterious effects and contribute to lithium triborate having a high damage threshold. These characteristics also allow tight focusing of high-duty-cycle radiation into lithium triborate.

#### *10-Hz Laser System*

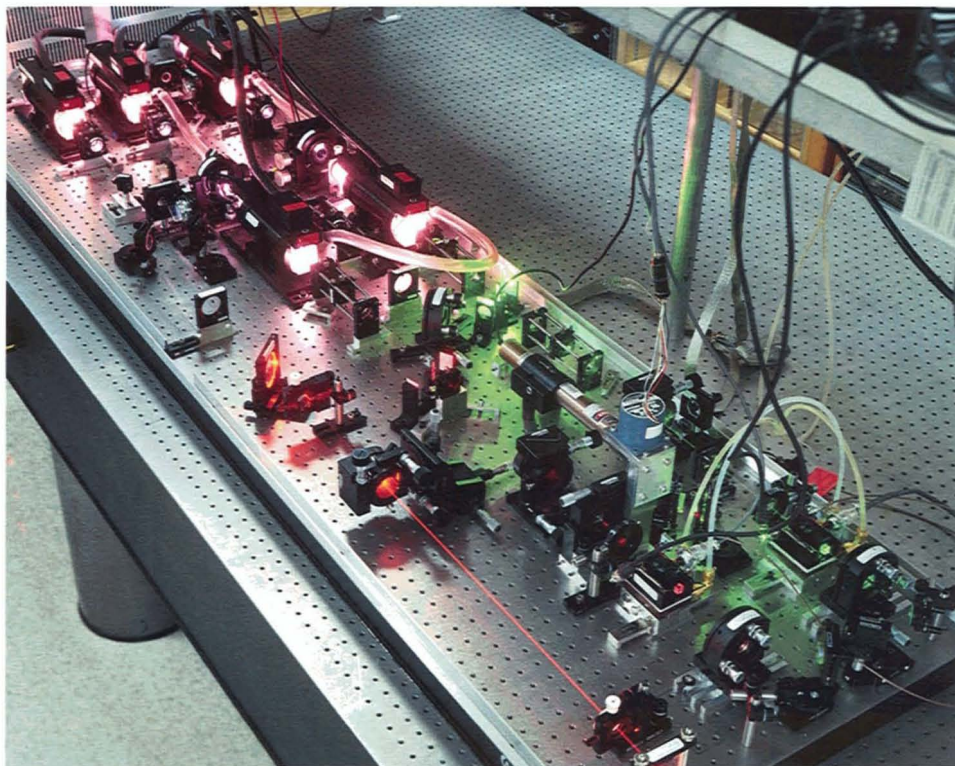
A schematic and photograph of the 0.5-J, 10-Hz source of sodium-resonance radiation is shown in Figure 10. Each 1.5-m-long oscillator consisted of a flat partial reflector, a flash-lamp-pumped Nd:YAG rod, a beam-expanding telescope (for greater mode filling of the Nd:YAG rod), a dielectric polarizer, a 0.5-cm-long antireflection-coated lithium-iodate crystal, an acoustooptic mode locker, and a 100% reflector with a 7-m radius of curvature. An intracavity aperture restricted laser oscillation to the  $\text{TEM}_{00}$  cavity mode for both Nd:YAG lasers. The 1.32- $\mu\text{m}$  laser cavity contained a dichroic mirror (transmission at 1.32  $\mu\text{m}$  and reflection at 1.06  $\mu\text{m}$ ) for the suppression of 1.06- $\mu\text{m}$  parasitic laser oscillation.

The 1.06- $\mu\text{m}$  oscillator emitted 160 mJ per macropulse at a 10-Hz rate, and the 1.32- $\mu\text{m}$  oscillator emitted 110 mJ per macropulse at the same rate. The 1.06- $\mu\text{m}$  and 1.32- $\mu\text{m}$  macropulses were synchronous. Each macropulse had a duration of 100  $\mu\text{sec}$  and consisted of a train of mode-locked micropulses each lasting 0.7 nsec and spaced at intervals of 10 nsec.

A single-frequency source drove the acoustooptic mode



(a)



(b)

**FIGURE 10.** The 0.5-J, 10-Hz laser source of sodium-resonance radiation: (a) schematic and (b) photograph of the laser system.

lockers, which phase-locked the micropulses for both laser oscillators. The relative phase of the mode-locker drive signals was adjusted to ensure that the micropulses from the 1.06- $\mu\text{m}$  and the 1.32- $\mu\text{m}$  lasers arrived in the sum-frequency-mixing crystal at the same time. The micropulses were transform-limited; i.e., they had a spectral width of about 1.5 GHz. In general, for circularly polarized sum radiation, such conditions result in efficient optical pumping to the sodium  $F = 2$  hyperfine state.

We have found that the temporal overlap of the initial relaxation oscillation (the large spike in Figure 11[a]) from either Nd:YAG laser with any part of the other laser pulse is very likely to result in damage to the sum-frequency-mixing crystal. Therefore, the output of the 1.06- $\mu\text{m}$  laser oscillator was passed through a Pockel's cell, which eliminated the first, and only, relaxation oscillation on the laser pulse. Because the 1.32- $\mu\text{m}$  laser pulse had an initial relaxation oscillation, the pulse was timed to precede the 1.06- $\mu\text{m}$  pulse slightly, thus preventing the 1.32- $\mu\text{m}$  relaxation oscillation from overlapping in time with the 1.06- $\mu\text{m}$  radiation. Figures 11(a) and 11(b) respectively show the temporal profiles of the laser macropulses and micropulses.

As shown in Figure 10(a), the 1.06- $\mu\text{m}$  radiation then passed through a beam expander and a Nd:YAG amplifier. After amplification, the 1.06- $\mu\text{m}$  laser pulse had an energy of 1 J. The output of the 1.32- $\mu\text{m}$  laser oscillator was amplified in a two-stage amplifier. The 1.32- $\mu\text{m}$  radiation passed directly into a beam expander and then passed twice through the first-stage Nd:YAG amplifier. The radiation then traveled through a 90° polarization-rotator quartz crystal to compensate for the thermally induced birefringence that occurred during the two stages of amplification. Next the laser beam was reexpanded and passed twice through the second-stage Nd:YAG amplifier. The first-stage amplifier was operated near the small-signal limit and produced a gain of about four; the second stage was operated closer to saturation and provided a gain of two. After amplification the 1.32- $\mu\text{m}$  laser radiation had an energy of 0.8 J.

The 1.06- $\mu\text{m}$  and 1.32- $\mu\text{m}$  radiation then passed through 0.5-m cylindrical lenses and were combined onto a common beam path by the dichroic mirror. The cylindrical lenses focused the laser radiation into the nonlinear crystal in the direction of lowest angular sensi-

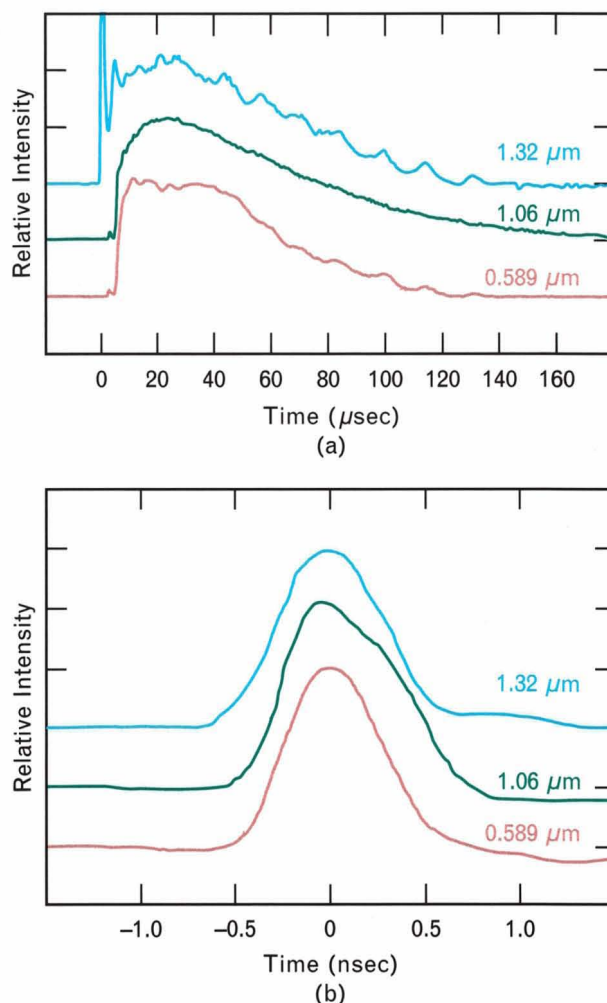
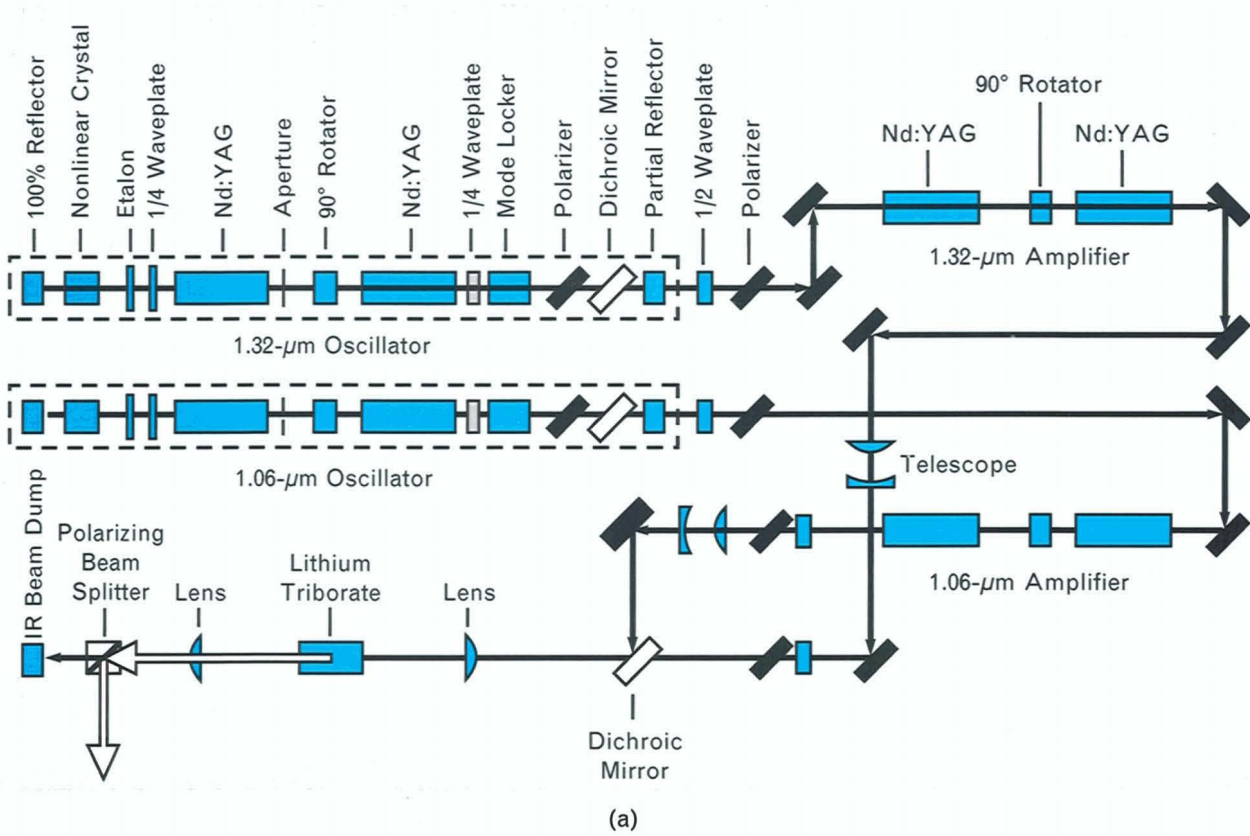


**FIGURE 11.** The 10-Hz laser system: (a) Temporal profiles of 1.32- $\mu\text{m}$ , 1.06- $\mu\text{m}$ , and 0.589- $\mu\text{m}$  laser macropulses. Note that the first relaxation oscillation of the 1.32- $\mu\text{m}$  laser continues above the top of the graph and is actually twice as high as shown. The initial relaxation oscillation of the 1.06- $\mu\text{m}$  laser has been substantially suppressed by a Pockel's cell. (b) Temporal profiles of the laser micropulses. The asymmetry of the 1.06- $\mu\text{m}$  micropulse is the result of intracavity second-harmonic generation, which stretches the laser micropulse.

tivity, which kept the infrared energy within the phase-matching acceptance angle. Focusing 1.0 J of 1.06- $\mu\text{m}$  radiation and 0.8 J of 1.32- $\mu\text{m}$  radiation into a 3-mm  $\times$  0.1-mm area in a 2-cm-long lithium-iodate crystal generated as much as 0.5 J of near-diffraction-limited sodium-resonance radiation.

The spectral envelope of the sodium-resonance radiation has a FWHM of 1.5 GHz, which consists of a comb of frequencies spaced at intervals of 100 MHz. This frequency interval is too large to excite all of the meso-



(b)

**FIGURE 12.** The 24-mJ, 840-Hz laser source of sodium-resonance radiation: (a) schematic and (b) photograph of the laser system.

spheric sodium atoms efficiently. But phase modulation of the 1.06- $\mu\text{m}$  and/or 1.32- $\mu\text{m}$  laser radiation should enable the generation of sidebands spaced at intervals of 10 MHz on each of the fundamental frequencies. The sidebands would allow access to all of the sodium atoms [21].

The 10-Hz laser system is currently being used to investigate the effect of laser linewidth, tuning, and polarization on the performance of the sodium beacon and to study the influence of radiation pressure, optical pumping, and saturation on the backscattered intensity from the sodium layer. Although this laser system has a repetition rate that is too low to be used for continuous adaptive optics compensation, the system is suitable for pulsed compensation.

#### *840-Hz Laser System*

A schematic and photograph of the 24-mJ, 840-Hz laser system is shown in Figure 12. Except for the much lower peak powers, much higher average powers, and much higher thermal loads on the Nd:YAG rods, this laser system is very similar to the 10-Hz system.

As previously discussed, the lower peak powers required tighter focusing into the nonlinear mixing crystal to achieve peak intensities sufficient for efficient frequency mixing. The tighter focusing combined with the higher average power of the 840-Hz laser system resulted in very-high-average-energy fluences in the nonlinear crystal. The much higher average thermal load on the Nd:YAG laser rods resulted in strong thermally induced refraction and birefringence in the rods. The laser oscillators and, to a lesser extent, the amplifiers were very sensitive to changes in the level of thermal loading. Small variations in thermal loading caused by aging of the flash lamps or variation in the drive current resulted in a large variation in the output power and beam quality of the laser oscillators. Because of this sensitivity of the laser system, it was difficult to obtain the maximum level of sum radiation power on a consistent basis.

The 1.06- $\mu\text{m}$  oscillator emitted 24 mJ per macropulse at a 840-Hz rate, and the 1.32- $\mu\text{m}$  oscillator emitted 14 mJ per macropulse at the same rate. Each macropulse had a duration of about 60  $\mu\text{sec}$  and consisted of a train of mode-locked micropulses lasting about 0.4 nsec

and spaced at intervals of 10 nsec. After amplification the 1.06- $\mu\text{m}$  laser beam had an energy of 54 mJ per pulse while the 1.32- $\mu\text{m}$  laser beam had an energy of 24 mJ per pulse.

The laser beams were made coaxial by a dichroic mirror and then focused by a 15-cm spherical lens into a 19-mm-long lithium-triborate crystal (Figure 13). The lens focused the input radiation to a  $1/e^2$  minimum diameter of about 100  $\mu\text{m}$ . When phase matched at a temperature of about 43°C, the lithium-triborate crystal was able to generate as much as 24 mJ of sum radiation per laser pulse (20 W of average sodium-resonance radiation). This output corresponds to an average mixing efficiency of 30% of the total Nd:YAG laser radiation and a 45% average mixing efficiency of the 1.32- $\mu\text{m}$  radiation. The peak mixing efficiency was substantially higher than the average mixing efficiency because of both temporal and spatial mismatch of the 1.06- $\mu\text{m}$  and 1.32- $\mu\text{m}$  laser beams. Figure 14 plots the sum radiation power and mixing efficiency as a function of the total input Nd:YAG laser power. The higher repetition rate of this laser system should allow its use in a continuous adaptive optics system.

#### **Summary**

We have developed both a 0.5-J, 10-Hz and a 24-mJ, 840-Hz laser source of sodium-resonance radiation suitable for the generation of a mesospheric sodium beacon for either a pulsed or continuous adaptive optics system. Both laser systems have achieved average mixing efficiencies of about 30%. The mixing efficiencies were limited by the relatively poor spatial and temporal overlap of the 1.06- $\mu\text{m}$  and 1.32- $\mu\text{m}$  laser beams.

Future development of this technology will be based on the use of diode-laser arrays to pump the Nd:YAG lasers. Much better mixing efficiencies at even higher powers are possible with diode-laser pumping instead of flash-lamp pumping because the former produces less thermal load on the Nd:YAG, and hence better spatial beam quality is possible. Since diode lasers can operate with a controlled temporal profile, better temporal beam quality of the Nd:YAG lasers is also possible. In addition, the reduction in energy consumption, decrease in electrical and light pollution, and small size of a diode-pumped laser system are important factors in the use of such a system at an astronomical facility.

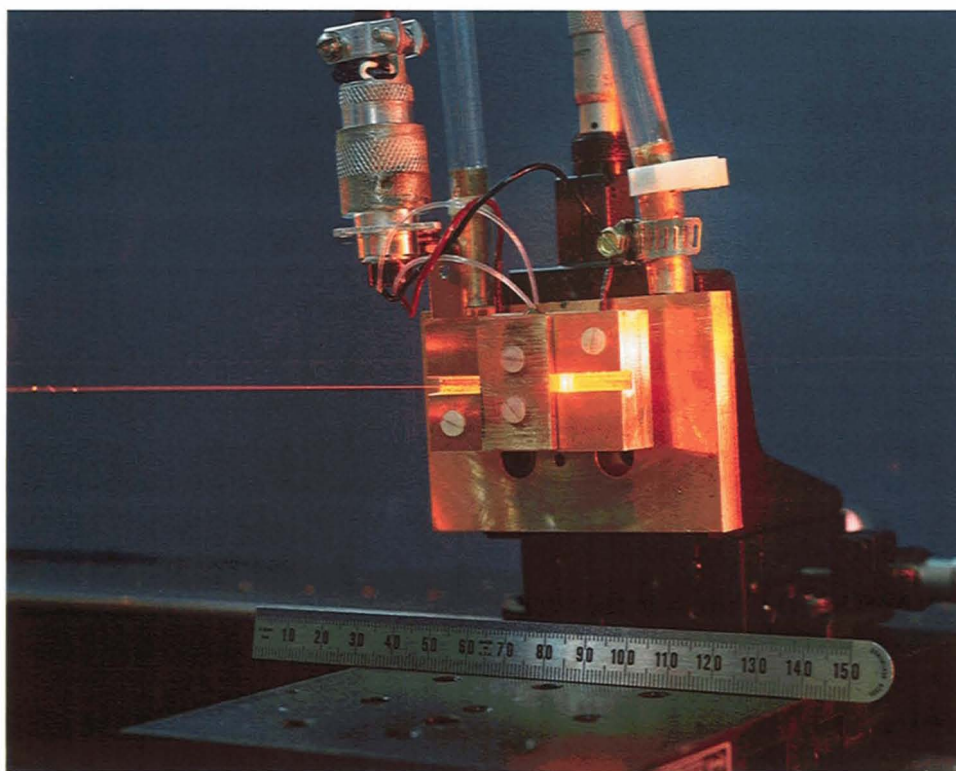


**FIGURE 13.** Photograph of the generation of sodium-resonance radiation in a temperature-controlled lithium-triborate crystal. The Nd:YAG laser beam (invisible) enters from the right and the sodium-resonance radiation (yellow) exits to the left. The weak yellow beam on the right is a result of a reflection of the main yellow beam by the rear surface of the uncoated nonlinear crystal.

**Acknowledgments**

The author gratefully acknowledges his collaborators A. Brailove and W.E. DeFeo for assistance with an early prototype laser system that was used to observe the mesospheric sodium layer; L. Bradley, P. Kelley, and R. Temkin for discussions on the characteristics of sodium excitation by a coherent train of resonant light pulses; C. Dill for construction of a jig for damage-proof installation of the metal sleeves onto the 840-Hz laser rods; T. Hotaling for development of the electronics necessary for the operation of these lasers; J. Korn for assistance in the development of the 10-Hz and 840-Hz laser systems; M. MacInnis for assistance in the maintenance of these lasers, the construction of various components, the repolishing of damaged nonlinear crystals, and the acquisition of leak-proof O-rings for the 840-Hz laser system; N. Menyuk for help with nonlinear crystals and for the suggestion to use lithium triborate with the

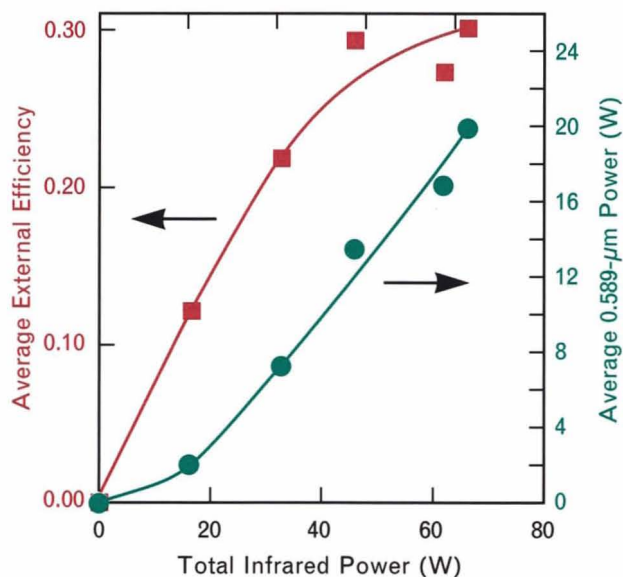


**FIGURE 14.** Sum-frequency power and efficiency as a function of input Nd:YAG laser power for the 840-Hz laser system.

840-Hz laser system; A. Mooradian for conception of the idea to generate sodium-resonance radiation through sum-frequency mixing of Nd:YAG laser radiation; and K. Wall for assistance in the development of the 840-Hz laser system.

This work was supported by the Air Force Phillips Laboratory and the Army Strategic Defense Command.

## REFERENCES

1. F. Merkle, P. Kern, P. Léna, F. Rigaut, J.C. Fontanella, G. Rousset, C. Boyer, J.P. Gaffard, and P. Jagourel, "Successful Tests of Adaptive Optics," *The Messenger* 58, 1 (1989). P. Kern, F. Rigaut, P.J. Léna, F. Merkle, and G. Rousset, "Adaptive Optics Prototype System for IR Astronomy II: First Observing Results," *Proc. SPIE* 1237, 345 (1990).
2. J.M. Beckers, F.J. Roddier, P.R. Eisenhardt, L.E. Goad, and K.-L. Shu, "National Optical Astronomy Observatories (NOAO) Infrared Adaptive Optics Program I: General Description," *SPIE* 628, 290 (1986).
3. R. Foy and A. Labeyrie, "Feasibility of Adaptive Telescope with Laser Probe," *Astron. Astrophys.* 152, L29 (1985).
4. L.A. Thompson and C.S. Gardner, "Experiments on Laser Guide Stars at Mauna Kea Observatory for Adaptive Imaging in Astronomy," *Nature* 328, 229 (16 Jul. 1987).
5. C.A. Primmerman, D.V. Murphy, D.A. Page, B.G. Zollars, and H.T. Barclay, "Experimental Demonstration of Atmospheric Compensation Using a Synthetic Beacon," submitted to *Nature*.
6. R.A. Humphreys, C.A. Primmerman, L.C. Bradley, and J. Herrman, "Atmospheric-Turbulence Measurements Using a Synthetic Beacon in the Mesospheric Sodium Layer," submitted to *Opt. Lett.*
7. D.L. Fried, "Optical Resolution through a Randomly Inhomogeneous Medium for Very Long and Very Short Exposures," *J. Opt. Soc. Am.* 56, 1372 (1966).
8. L. Goad and J. Beckers, "A Near Infrared Astronomical Adaptive Optics System," *SPIE* 1114, 73 (1989).
9. J.W. Hardy, "Active Optics: A New Technology for the Control of Light," *Proc. IEEE* 66, 651 (1978).
10. R.R. Parenti and R.J. Sasiela, "Laser Guide-Star Systems for Astronomical Applications," to be published.
11. J.C. Twichell, B.E. Burke, R.K. Reich, W.H. McGonagle, C.M. Huang, M.W. Bautz, J.P. Doty, G.R. Ricker, R.W. Mountain, and V.S. Dolat, "Advanced CCD Imager Technology for Use from 1 to 10000 Å," *Rev. Sci. Instrum.* 61, 2744 (1990).
12. C.S. Gardner, B.M. Welsh, and L.A. Thompson, "Design and Performance Analysis of Adaptive Optical Telescopes Using Laser Guide Stars," *Proc. IEEE* 78, 1721 (1990).
13. E. Arimondo, M. Inguscio, and P. Violino, "Experimental Determinations of the Hyperfine Structure in the Alkali Atoms," *Rev. Mod. Phys.* 49, 31 (1977).
14. C.S. Gardner, D.G. Voelz, C.F. Sechrist, Jr., and A.C. Segal, "Lidar Studies of the Nighttime Sodium Layer over Urbana, Illinois—1. Seasonal and Nocturnal Variations," *J. Geophys. Res.* 91A, 13659 (1986).
15. K.H. Fricke and U. von Zahn, "Mesopause Temperature Derived from Probing the Hyperfine Structure of the D<sub>2</sub> Resonance Line of Sodium by Lidar," *J. Atmos. Terr. Phys.* 47, 499 (1985).
16. *U.S. Standard Atmosphere, 1976*, National Oceanic and Atmospheric Administration, National Aeronautics and Space Administration, and the U.S. Air Force, Washington (Oct. 1976), pp. 91–92.
17. B.M. Welsh and C.S. Gardner, "Nonlinear Resonant Absorption Effects on the Design of Resonance Fluorescence Lidars and Laser Guide Stars," *Appl. Opt.* 28, 4141 (1989).
18. O. Svelto, *Principles of Lasers*, 2nd ed. (Plenum Press, New York, 1982), p. 60.
19. D. Hils, W. Jitschin, and H. Kleinpoppen, "Production of a Highly Polarized Sodium Atomic Beam," *Appl. Phys.* 25, 39 (1981).
20. L.C. Bradley, "Atomic Excitation by a Pulse Train I: Two-Level Atoms"; "Atomic Excitation by a Pulse Train II: Sodium," *Optical Society of America Ann. Mtg., Tech. Digest, Boston, 4–9 Nov. 1990*, Papers TuE5 and TuE6. "Pulse-Train Excitation of Sodium for Use as a Synthetic Beacon," to be published.
21. T.H. Jey, "Sum Frequency Mixing of Frequency Modulated Laser Radiation," *Conf. on Lasers and Electro-Optics, Baltimore, 24–28 Apr. 1989*, Paper THN3.
22. P. Strohmeier, T. Kersebom, E. Krüger, H. Nölle, B. Steuter, J. Schmand, and J. Andrä, "Na-Atom Beam Deceleration by a Mode-Locked Laser," *Opt. Comm.* 73, 451 (1989).
23. T.H. Jey, A.A. Brailove, and A. Mooradian, "Sum Frequency Generation of Sodium Resonance Radiation," *Appl. Opt.* 28, 2588 (1989).
24. T.H. Jey, "Suppression of Laser Spiking by Intracavity Second Harmonic Generation," *Appl. Opt.* 30, 1011 (1991).
25. N. Menyuk and J. Korn, "Thermal and Absorptive Properties of LiB<sub>3</sub>O<sub>5</sub>," *Solid State Research Report*, Lincoln Laboratory, MIT (1990:1), DTIC #AD-A225803, p. 18.



**THOMAS H. JEYS**

is a staff member in the Quantum Electronics Group, where his focus of research has been in laser development for adaptive optics applications. Before joining Lincoln Laboratory five years ago, Tom was an assistant professor at Rice University. He received the following degrees in physics: a B.S. and an M.S. from the University of Houston, and a Ph.D. from Rice University.